ISSN 0915-633X

# NATIONAL INSTITUTE FOR FUSION SCIENCE

## Steady State Tests of High Voltage Ceramic Feedthoughs and Co-Axial Transmission Line of ICRF Heating System for the Large Helical Device

T. Mutoh, R. Kumazawa, T. Seki, F. Simpo,
G. Nomura, T. Ido and T. Watari

(Received - June 11, 1998 )

NIFS-552 June 1998



RESEARCH REPORT
NIFS Series

NAGOYA, JAPAN

# STEADY STATE TESTS OF HIGH VOLTAGE CERAMIC FEEDTHROUGHS AND CO-AXIAL TRANSMISSION LINE OF ICRF HEATING SYSTEM FOR THE LARGE HELICAL DEVICE

TAKASHI MUTOH, RYUHEI KUMAZAWA, TETSUO SEKI, FUJIO SIMPO, GORO NOMURA, TSUYOSHI IDO and TETSUO WATARI
National Institute for Fusion Science, 322-6 Oroshi-cho, Toki-shi, 509-5259, Japan

JEAN-MARIE NORTERDAEME
Max Planck Institute for Plasma Physics, D-85748 Garching, Germany

## ABSTRACT

Steady state Ion Cyclotron Range of Frequency (ICRF) heating technologies have been developed to heat plasma for more than 30 minutes in the Large Helical Device (LHD). Steady state operation tests of high voltage up to 40 $kV_{0P}$ for more than 30 minutes were carried out on the RF vacuum feedthroughs and the co-axial transmission line in the test set. Four types of ceramic feedthroughs each having a diameter of 240 mm were tested. The cone-type alumina ceramic and the cylinder-type silicon nitride composite-ceramic feedthroughs produced good performances of 40 kV/30 minutes and 50 kV/10 seconds. The others had vacuum leaks when subjected to a long pulse duration. The temperature of the cone-type alumina ceramic feedthrough was measured during the ICRF operations. By using gas-cooling techniques, the temperature increase of the ceramic was substantially reduced and saturated within 20 minutes. Without any gas-cooling techniques, the temperature increased linearly and did not saturated. Therefore, this approach could not be used for steady state operation. The RF dissipation on the ceramic was calculated using the finite element computer code (ANSYS). It was found that damaged feedthroughs had local high heat spots, which could result in vacuum leaks. A water-cooled co-axial transmission line of 240 mm diameter was designed and tested for steady state operation. The specially designed connector components and Teflon insulator disks were tested. During the test operation, the insulation gases of nitrogen, sulfur hexafluoride and carbon dioxide were used to compare the capability of insulation for steady state. For the duration of a 10-second pulse, these gases performed well up to 60 $kV_{0P}$. However, for steady state operation, carbon dioxide gas could not withstand voltages above 40 $kV_{0P}$. The connector components of the transmission line performed without problems below 50 $kV_{0P}$ and 1 $kA_{0P}$ for a 30-minute steady state operation. The performance of the feedthroughs and transmission line exceeded the specifications for steady state heating in the LHD.

Keywords: ICRF, steady state heating, LHD, ceramic feedthrough, co-axial transmission line, insulation gas

## I. INTRODUCTION

The ICRF heating system is prepared for a steady state heating source in the LHD[1,2,3]. The LHD has superconducting windings and can sustain steady state high temperature plasma. ECH heating is foreseen as the main source for the production and heating of steady state plasma. During the first phase of the experiment with the LHD, the steady state ICRF heating of 3 MW is scheduled. There is a general misconception that ICRF heating devices are well developed for high power and long pulse duration. However, it is not easy to obtain a high power system of more than 1 MW in steady state conditions. The frequency range of the LHD ICRF is 25-100 MHz. A similar frequency band is also used at RF transmitter broadcast stations. However, the output power class of a broadcast transmitter does not refer to the average power, but to the peak power value of the AM modulation. Therefore, the steady state operation of a Mega Watt class is truly an advanced research.

Much research has been carried out to understand clearly the steady state ICRF system in the LHD[4,5,6,7,8]. In the test equipment setup for the LHD ICRF system, all main components were tested for the purpose of developing the steady state RF technologies. The test equipment included transmitters, transmission line, a DC break, an impedance matching circuit, a vacuum ceramic feedthrough, a test loop antenna and a vacuum chamber. By using the realistic test equipment, the performance of the component design was confirmed over the frequency range of 45-50

MHz.

In the ICRF system, ceramic feedthrough is used for vacuum sealing of the feeder line. This enables the RF power to the antenna launcher to be introduced at the entrance of the plasma vacuum chamber. It has to withstand the high RF voltage or the large RF current due to the presence of the large Voltage Standing Wave Ratio (VSWR). For the LHD, it is estimated that the RF voltage on the feedthrough section is between 30 ~ 40 kV. In the case of antennas, which contain a resonant circuit in order to increase the input impedance, there is a decrease in VSWR as well as RF voltage at the feedthrough. However, even in such circumstances, the antenna has to take care of the fast load changes that cause high RF voltages on the feeder lines.

The ceramic feedthroughs for ICRF heating devices have been developed in major laboratories. There are reports on the feedthroughs of original design developed in France, PPPL[9] and ORNL[10,11] in USA, Garching[12] in Germany and JAERI[13] in Japan. These feedthroughs have operated reasonably well in this application. However, they are designed for pulse operation. Even if the feedthroughs are designed for long pulse duration, there are no test records available exceeding more than a few minutes. It is predicted that for large toroidal devices such as ITER, ICRF systems will need to operate for more than an hour. In the LHD, it is planned to carry out the multi Mega Watt ICRF heating tests for more than 30 minutes. This is the main purpose of this development and the steady state test of feedthroughs. The basic shapes of the tested ceramic have partially come from the above laboratories. However, they have been largely modified to increase the stand off voltage and to add cooling channels for steady state operation. With the advanced option for the feedthrough design, attempts have been made to use silicon nitride composite ceramic to increase the thermal shock strength and the mechanical strength compared with that of alumina ceramic. In addition, the O-ring seal method has been tried instead of a brazed seal. This paper covers the steady state operation test for more than 30 minutes using several types of ceramic feedthroughs.

Another important component is an RF co-axial transmission line in large VSWR and high RF voltage section between the low impedance antenna and the first matching stub tuner. Water-cooled co-axial transmission lines were developed having a high stand off voltage for the steady state operation. To withstand the high RF voltage of over 40 kV, a large diameter co-axial transmission line of 240 mmϕ and characteristic impedance of 50 Ohm was designed. To increase the stand off voltage of the co-axial line, the shapes of the insulator Teflon plate and conductor were redesigned and tested. The original design of the Teflon spacer having under-cut recess structure was proposed by the JAERI group[14]. This concept is used on the LHD transmission line.

A high RF voltage test was conducted to examine several kinds of gas-filled insulation within the transmission line. Until now, some reports have produced similar test results to those carried out in the pulse operation[15]. In this paper only the steady state operation tests are reported, giving comparison of insulation gas species. These results are the first trial within this frequency range.

In section II, the experimental setup of the ceramic feedthrough and transmission line tests are described. In section III, the steady state and high RF voltage test results of the ceramic feedthroughs are described. The results are compared with the calculation produced using the ANSYS finite element code in section IV. In section V, the results of the co-axial transmission line with various kinds of insulation gases are reported.

## II. EXPERIMENTAL SETUP FOR THE DEVELOPMENT OF THE STEADY STATE RF COMPONENTS

In the past, many ICRF system components have been designed and tested operating at high voltage for a long duration. The test equipment we used consisted of a 1.5 MW steady state RF transmitter, a co-axial transmission line of 240 mmϕ, an impedance matching circuit, a ceramic feedthrough, test antenna and test vacuum chamber. The layout is shown in Fig.1. The transmitter output power exceeds 1.5 MW for steady state over a frequency range from 25-100 MHz. The steady state operation test of the transmitter at 50 MHz, 1.6 MW and 5000 seconds was achieved by using a very large dummy load[7]. For the antenna and the feedthrough tests, the transmission line was terminated by the R & D antenna loop inside a test vacuum chamber. The first stub tuner (antenna side) for impedance matching is the liquid stub tuner, which was originally developed for the previous test equipment[7]. The contact finger type created difficulties for steady state operation and therefore the first stub tuner was changed for a new type of tuner. When using the liquid tuner, the electric length can be changed even during the RF operation. The liquid dielectric substance is silicon oil with low vapor pressure. The test pieces of the ceramic feedthrough and the co-axial transmission line were placed

in this circuit. There was no artificial dummy load in the circuit. For this reason, the VSWR between the antenna loop and the first stub tuner (liquid stub tuner) is very large. (Of the order of 200 due to the low loss resistance.)

For low circuit resistance, the peak voltage of the transmission line $V_{max}$ is approximated by the following equation:

$$V_{max} = (Z_0 \times \rho \times \text{Power})^{0.5} \quad (1)$$

where $\rho$ is the VSWR on the transmission line between the antenna loop and the first-matching stub tuner and $Z_0$ is the characteristic impedance of the co-axial line. To test the circuit at 40 kV peak voltage, the required RF power was less than 200kW. For the feedthrough test, the pre-matching stub was used to reduce the voltages of the transmission line and therefore to focus the test objects on the feedthrough. However, in the case of the transmission line test, the co-axial transmission line was terminated at point A in Fig.1. Several insulator plates were placed near the peak RF voltage position.

The transmission line has a diameter of 240 mm to prevent the RF breakdown. It is filled with insulating gas at 0.4 MPa (3 atmospheric pressure by gauge). A strong cooling system is used for steady state operation. All the inner conductors of this circuit are designed so that circulating water flows inside the antenna strap and the return conductor, the co-axial feeder line, the ceramic feedthrough, the matching stubs, and the transmission line. Two kinds of the water inlet/outlets are used. One is the shorted end of the impedance tuning stubs and the another is the insulator pipe at L- or T-junction. The test set of Fig.1 has eight inlet/outlet channels for inner conductor cooling. Two channels operate through the tuning stubs and six channels through insulator pipes. The outer conductors are also cooled through the outside water jackets.

## III. STEADY STATE AND HIGH VOLTAGE TESTING OF CERAMIC FEEDTHROUGHS

In RF heating systems in fusion experimental devices, the vacuum insulation of the transmission line presents a problem especially for the long pulse duration. In the ICRF frequency range, alumina ceramic is used for the vacuum insulating materials. Through the ceramic sealing, RF power is fed into the discharge chamber from the insulating gas-filled transmission line. In the research and development case, the pressure difference between each side of the ceramic disk rises to 0.4 MPa(4 kg/cm$^2$). The diameter of the LHD feedthrough is 240 mm; therefore, the total pressure driven force is estimated to be about 1.5 tons on the ceramic disk. In tokamaks, the electromagnetic force is added to this value, but fortunately there is no quick disruption in the LHD.

In the LHD, it is planned that more than 1 MW of ICRF power will be injected for more than 30 minutes through one feedthrough to the plasma. By assuming the plasma coupling resistance of 5 Ohm at 50 Ohm characteristic impedance of co-axial line, in the worst case, the ceramic feedthrough must withstand an RF voltage of up to 32 kV(o-peak). It can be reduced by the correct positioning of the feedthrough along the transmission line. However, to maintain the options for the use of a wide frequency range for optimizing the experimental program, the feedthrough, hopefully, can withstand 40 kV for CW operation. The RF electric field on the ceramics is dissipated by dielectric loss due to the finite value of tan$\delta$. It is several hundred Watts in the ceramic disks at 40 kV. For a long pulse duration of more than several minutes, thermal stress and pressure driven force can cause severe problems such as a vacuum leak or discharge within the vacuum. In future experimental devices such as ITER, ICRF heating/current drive should operate for an extended period of a number of hours. To complete the steady state ICRF system, it is essential to develop the ceramic feedthrough.

Five different kinds of ceramic feedthroughs, which were originally designed for the LHD, were tested. The outer diameter of all feedthroughs is 240 mm and the inner conductor diameter at the connection point is 102 mm. These sizes are considerably larger than the usual ICRF feedthroughs. The drawings in Fig.2 shows the cross section of the tested feedthroughs, which all have a water-cooled inner conductor. The crank type and disk type have simple cylindrical inner conductors. Similar to the disk type, two slightly different types were tested of which one has cooling channels inside the ceramics while the other has no channels, as shown in Fig.2. These crank and disk types have a simple shape of inner and outer conductors including corona rings to reduce the electric field at the brazing points. Due to the simple shape of the inner and the outer conductors, the sizes, weight and costs are relatively small in comparison with the cone and cylinder types.

The shape of ceramics of the cone type is similar to that of the Princeton (PPPL) type feedthroughs. The LHD cone-type feedthrough of this experiment has a large diameter to withstand the high RF voltage and includes the forced gas-cooling channels in order to remove the dielectric heat loss in the ceramic material. The insulation gas was injected into the ceramic surface through eight outer

nozzles. To prevent a temperature rise in the ceramic, $SF_6$ or nitrogen gas was passed through the nozzles at a rate of up to 330 liter/minute at 0.4 MPa. The temperature of the ceramic was measured using an IR thermometer inserted in a small port, as shown in the figure.

The ceramics of the above three types are made with alumina ($Al_2O_3$ 99%) and these are brazed with Kovar (Fe,Co,Ni) alloy to achieve vacuum sealing. However, the cylindrical type feedthrough is made of silicon nitride ($Si_3N_4$) composite ceramics and has an O-ring type vacuum seal and, therefore, does not require a brazed seal. The ASDEX ICRF group, who used alumina ceramics[12], also reported the feedthrough design that does not use brazing. The silicon nitride ceramic composite of the cylinder type uses the same material as that used in microwave windows of ECH system in the LHD[16]. The dielectric tangent loss of the $Si_3N_4$ composite is very low, in the order of $10^{-4}$ and the thermal stress characteristic is very strong ,similar to that of the usual $Si_3N_4$ ceramics. In this type, it is not necessary to be concerned about the thermal cracks that cause the vacuum leak.

The RF tests of the feedthroughs were performed in the test chamber with the R& D antenna. The feedthroughs were located near the highest voltage position between the antenna and the tuners. The test results are summarized in Fig.3. The tested maximum RF voltages are shown in the horizontal axis by two kinds of rectangles. The black rectangles show data for the 30 minutes of operation whereas the white ones are data for a ten-seconds operation. There is no good data for the crank type or disk types compared with the other two types. Two types of the disk ceramics were tested. One type (Disk1) has a cooling duct inside the ceramic using fluorinate (FC75) as coolant liquid to control the ceramic temperature. Another type (Disk2) has no cooling channel. The crank and the disk types suffered serious damage due to the thermal stresses which resulted in vacuum leaks at the brazed sections. The vacuum leak occurrences are illustrated by asterisks in the figure. The RF duration time of these events is also shown. These problems occurred during the transition to higher voltage and the longer time of operation. All vacuum leaks experienced, occurred at the brazed points between the ceramic and Kovar alloy. As a result, the crank and disk types could not sustain RF voltages over 30 kV for more than several minutes.

In the case of the cone and the cylinder types, high RF voltages of the order of 40 kV were achieved for long operational times of 30 minutes. These operational limits are determined by the rise in vacuum pressure in the test vacuum chamber and not by the feedthrough performances. The feedthroughs were connected to the test antenna inside the chamber and the RF power was finally dissipated onto the chamber wall and the antenna components. Part of the losses dissipated on to the antenna were removed by cooling water, but these heat losses caused a rise in vacuum pressure in the chamber which finally led to RF discharge in the chamber. The RF discharge caused a large and rapid impedance change, which could not be recovered by impedance matching using frequency feedback control. Both types of feedthroughs can withstand RF voltages of the order of 40 kV for a duration longer than 30 minutes without RF breakdown or vacuum leaks during the experiments. It was concluded, as seen in Fig.3, that the cone type and the cylinder type can be used for steady state operation system.

Photographs of the cone-type and cylinder-type feedthroughs are shown in Fig.4. Figure 4(a) is the cone type feedthrough having eight gas injection nozzles around the outer conductor. Throughout the experiment, as shown in Fig.3, the sulfur hexafluoride($SF_6$) gas at 0.4 MPa, used as the insulation gas, was blown over the ceramic surface at about 40 liters/minute in order to cool the ceramic surface. Figure 4(b) shows the cylinder-type feedthrough, which consists of the silicon nitride composites' ceramic that has a dark colored surface. This type is demountable by using an O-ring seal method. Therefore, the ceramic, the inner conductor, and the Teflon spacer are shown separately. This picture was taken after the steady state experiment, as shown in Fig. 3; there was no damage to the ceramic surface. We did not use the helicoflex type metal O-ring to simplify the RF current path at the seal section. The steady state operation was carried out by using the viton O-ring seal.

After completing experiments shown in Fig.3, the first choice of the feedthrough for the LHD experiment was fixed onto the cone type. The manufacturing cost of the cylinder type was a little higher than the cone type, which was the reason for choosing the cone-type feedthrough. Research and development effort was now focused at the cone-type feedthrough. The temperature measurement during the RF test became available for the cone-type feedthrough by using an IR thermometer. The monitoring of the ceramic temperature was important in order to develop the steady state devices. It was particularly important to observe the time for temperature saturation after a number of hours. The increments in temperature of the ceramic surface after the 30 minutes of operation were measured by changing the RF voltage applied to the ceramic. The results were plotted, as shown in Fig.5(a). The cone-type feedthrough has a gas-cooling system.

Without gas cooling, the temperature increase exceeded a linear characteristic for a change in RF voltage between the inner and outer conductors. The temporal behavior does not show the saturation trend, therefore the increasing rate of the ceramic temperature depends on the heat dissipation in the ceramic. The power loss is relative to the dielectric loss of the RF field inside the ceramic material. The dielectric power loss is expressed by the following equation:

$$Q=\omega \varepsilon E^2 \tan\delta \qquad (2)$$

where, $\omega$ is frequency, $\varepsilon$ is dielectric constant, E is electric field strength and $\tan\delta$ the tangent loss. The heat loss depends on the square of the electric field and usually the tangent loss is an increasing function of the temperature. During the 30 minutes' operation, the temperature increase was almost linear without saturation in the case without gas cooling. The dependence on the electric field in Fig.5(a) is consistent with the square dependence in Eq.(2). The effect of the temperature dependence on the tangent loss is not clear.

The effect of the gas cooling was remarkable in the experiments. Ceramic temperature increments were measured by changing the gas flow rate, as shown in Fig.5(b). In this experiment, nitrogen gas was used instead of $SF_6$ gas used in the experiment of Fig.3. The temperature increments of the alumina ceramic were reduced from 26 to 13°C by increasing the gas flow rate from zero to 330 liter/min. The data obtained were at an RF voltage of 30 kV for a duration of 30 minutes with a flow rate from all eight injection nozzles. The increase was suppressed to half that of the non-additional gas cooling case.

The most noteworthy point is the saturation tendency during the 30 minutes of operation. The temporal behaviors of the temperatures with and without gas cooling were shown in Fig.6. Without gas cooling, the temperature increased almost linearly up to 30 minutes without any sign of saturation. This linear increase suggests that the time constant for heat conduction will be long, partly due to the temperature dependence of the dielectric loss constant. The dielectric loss-constant of alumina ceramics has a positive temperature dependence, which causes additional heat production for an increase in temperature. The positive feedback of the ceramic temperature is frequently observed in high power microwave systems such as the ECH system[16]. In the ECH window case, the heat loss positive feedback on the ceramic window leads to runaway phenomena, which cause serious damage. Therefore, the monotonic increase of the temperature is dangerous for components of a steady state device. However, by using the effective gas-cooling method, the temperature increase was suppressed into complete saturation, as shown in Fig.6. The time constant was about twenty minutes. The increase in temperature saturation suggests that the cone-type feedthrough method can be used for a long period of time. Therefore, the gas-cooling channels are an inevitable means for the cone-type alumina feedthrough.

## IV. CODE CALCULATION OF RF DISSIPATION IN CERAMICS

As shown in Fig.3, there were significant differences between the five feedthrough test results. The fatal vacuum leaks occurred with three feedthroughs at the brazing points of ceramic part. Before these sudden events occurred, no signs of impedance mismatching were observed, which imply that RF breakdown had taken place in the circuits. In addition, there were no traces of arcing on the surfaces of the broken feedthrough ceramics. The vacuum leaks occurred during the phase of temperature decay. When the three damaged types of feedthrough were operated, the RF pulse duration was extended step-by-step. At the same time, other components such as the transmitter tetrode and the test antenna in the vacuum chamber were tested. Because of this, the temperature of the feedthrough increased gradually from the room temperature. In the event of trouble occurring, the RF pulse was terminated immediately without going through the procedure of soft cool down. In such a case, the temperature decay phase was far more rapid than the warm-up phase. The vacuum leaks that had occurred, happened several minutes after the sudden RF shut down. From these observations, it was deduced that the leaks were caused by thermal stress at the brazed points.

To compare the test results with the evaluations of RF heat dissipation in the ceramics, the ANSYS finite element code was used to analyze the dissipation power distributions. In this calculation, it is assumed that the voltage change on the axis direction is negligible. Therefore, the TEM mode on the co-axial line has the same electric field pattern as the electrostatic field. In Fig.7, the dissipation power of the ceramics calculated by Eq.(2) is shown by the contour line plots. The calculation conditions are as follows. The RF voltage between conductors is 50 $kV_{0P}$, the frequency is 50 MHz, the dielectric constant ratio is 9.7 and the tangent loss is 0.0002. The dissipation power depends directly on the electric field strength. In the results shown in the figure, the electric field is strongest near the central conductor and at the point where the conductors are close together. This

applies particularly to the crank and disk types where the electric field is very strong near the central conductor. It can be seen that the RF heat dissipation in these components was relatively large. The field strength of the cone and cylinder type is smaller than other types, and depends mainly on the gap between conductors along the length of the ceramic surface. The dielectric constant ratio of the alumina ceramics is 9.7. Due to the large dielectric constant ratio, the trend of the contour lines of the electric field strength is to intersect with large angles with respect to the ceramic surface.

The calculation results are summarized in Table I. Peak power, means the dissipation power at the local maximum point. These points are located at the edge regions where the ceramics are brazed to the metal structures of inner and outer conductors. For the disk and crank types, the peak dissipation power exceeded 6 W/cm$^3$ and 3 W/cm$^3$, respectively. However, the dissipation power for cylindrical and cone types remains around 1 W/cm$^3$. In Table 1, the RF voltages are shown at which the vacuum leaking occurs. The presence of the high peak power and vacuum leaks occurred simultaneously in the experiments. This coincidence with vacuum leaks implies that the thermal stress could cause cracks in the brazed components, as well as the positions of high heat dissipation, which coincide with the positions of cracks in the ceramics. If there were no leaks, the recordings of the CW operation increased to around 40 kV for 30 minutes, as shown in Table 1. The experimental results can be explained by the ANSYS finite code calculations of the RF dissipation power on the ceramics as mentioned above.

## V. HIGH VOLTAGE AND STEADY STATE TEST OF THE CO-AXIAL TRANSMISSION LINE FOR THE LHD

For LHD ICRF heating, the power demand required to heat the plasma exceeds 1MW through one feedthrough port, assuming a plasma coupling resistance of 5 ohm. The characteristic impedance of the co-axial transmission line is 50 Ohm. Therefore, a large VSWR occurs between the antenna loop and the first stub tuner. The operation of 1 MW into 5 ohm plasma resistance causes a maximum RF voltage of the order of 32 kV on the transmission line. To withstand this high RF voltage for a long duration of time, the co-axial transmission line must have a large diameter of 240 mm. To remove RF heat loss in the line, cooling water must be circulated inside the center conductor.

During the high voltage RF tests, breakdowns occurred near the insulator section, and arc traces were found on the insulator disks on every occasion. Teflon plates were used in the co-axial lines for the insulator plate. Teflon is regarded as a highly suitable material for an RF insulator. Recently General Atomics and Oak Ridge National Laboratory groups made a similar test comparing various insulator materials[15]. From their tests, Teflon was also proved to be the most suitable material. During our experiments, if breakdown occurred in a long pulse test, serious damage resulted on the spacer. Based on many experiences, the design of the spacer is one of the most important issues to complete the high performance co-axial line. The RF breakdown is thought to be triggered locally by the point of the high intensity electric field. Experience has shown that it is usually the edge of the spacer holder of the conductors. To reduce the electric field strength at the corners along the Teflon insulator surface, the design concept, developed by JAERI ICRF group[14], was introduced.

The cross section of the newly designed straight co-axial transmission line for steady state and high voltage conditions is shown in Fig.8. To remove the heat loss on the center conductors, the circulating water flows inside the center conductors. The reduction optimization of the local electric field strength can be seen in the shape of the Teflon plates. On both sides of the spacer, undercuts are made to reduce the local electric field strength along the insulator surface. Small recess structure which keeps some space at the point of contact between the Teflon insulator and the edges of the inner or outer conductors are effective. These shapes are also shown in the enlarged drawing in Fig.8(b).

The connector parts were carefully designed to ensure that they were watertight and had reliability of electrical contact. It is very important to maintain watertight conditions inside such a closed electric circuit. For more than five years of test experiments, no water leaks have occurred through the connector O-rings. To ensure the electrical contact, the contact finger plates manufactured by the Multi-Contact Co. are used at each insertion point. The contact finger and the O-ring gasket are located in series at the insert pipe, as shown in Fig.8(b). The photograph of the inner and outer connectors is shown in Fig.9. The material of the outer conductor is aluminum, while the center conductor is silver coated copper. The holes in the Teflon insulator are used for gas circulation of the feedthrough cooling. The circulating water flowing inside the conductor is very effective to remove the heat loss from the RF dissipation in conductors and connectors. This cooling technique is an important key factor for the steady

state operation.

The high voltage and steady state test of the co-axial transmission line was performed at 40 MHz reduced to a short circuit at half the total length. The short circuit point is at point A, as shown in Fig.1. The reduced test circuit excluded the uncertainties of the feedthrough section and the antenna loop circuit inside the vacuum chamber. The length of the high VSWR line is about 8m. Three Teflon spacers were located near the points of highest voltage.

Usually, the transmission lines are pressurized by the insulating gas in order to increase the stand off voltage. For the insulating gas, three kinds of gas species were tested: sulfur hexafluoride ($SF_6$), carbon dioxide ($CO_2$) and nitrogen gas ($N_2$). These gases have been commonly used by many laboratories as the suitable insulating gas. However, there is no published data comparing the performance of these gases in the same experimental setup, as in the ICRF frequency range. In particular, the comparison of the insulation gas species were tested in both pulsed and the steady state operation.

The gas pressure was 0.4 MPa, which is the same condition as that of the LHD ICRF system. The results are shown in Fig.10. The tests were carried out in two different modes. The first was the pulse operation of ten second and the other was the steady state operation of 30 minutes. For the pulse operation, the test records of three species reached up to 60 kV. For $SF_6$ and $N_2$, there were no apparent difficulties in raising the RF voltage up to 60 kV without observing any indication of breakdown. However, when $CO_2$ gas was tested, breakdowns occurred while increasing the voltage to 60 kV. In the steady state operation mode, $CO_2$ gas appeared to have insufficient stand-off voltage capability. Break down was observed after several minutes at 40 kV of CW mode. Therefore, it was not possible to record data beyond two minutes of operation for the $CO_2$ gas case. On the other hand, good performance was recorded for both $SF_6$ and $N_2$ gases. In both gases, no breakdown was observed until 40 to 50 kV potential was reached, therefore the data shown in the figure is almost identical. The difference at the 30 minutes point is not due to breakdown. The tests were stopped because of the concern for the safety of the system.

In other experiments conducted, breakdown using $SF_6$ gas produced considerably dirty, decomposed products and toxic gas in a steady state mode when the arc detection system was incomplete. Therefore, it was concluded that nitrogen gas was the most favorable of the three tested gas species for the steady state experiments using Teflon insulator plates.

## VI. CONCLUSIONS

Steady state ICRF heating technology for the LHD has been developed. Several new types of ceramic feedthroughs and large diameter co-axial transmission lines were designed and tested. They were designed to introduce cooling water and to withstand high RF voltage for steady state operation. Two types of ceramic feedthroughs satisfied our required specifications and withstood potentials over 40 kV for more than 30 minutes. Cone-type feedthroughs having gas-cooling system were chosen for the LHD antenna system. Ceramic temperature of the cone type was measured by an IR thermometer. The time constant of the ceramic was longer than 30 minutes without gas cooling and gas cooling was necessary to saturate the temperature rise within the tolerable level for the steady state operation. By using a strong gas-cooling technique, the temperature rise of the ceramic surface was suppressed to 12 °C at the RF voltage of 30 kV. Another cylinder-type feedthrough having a silicon nitride composite ceramic and O-ring seal method without brazed seals also gave good performance.

The ceramic feedthrough experiments were compared with the ANSYS calculation code ,which evaluates the RF dissipation distribution in ceramics. The feedthroughs, which did not have good performance, had a high local dissipation power in the code calculations.

The co-axial transmission line using a large diameter of 240 mm and with a water cooling channel inside the inner conductor was newly designed and tested. With several kinds of insulating gas species, the performance was tested, and the stand off voltage of more than 40 kV for more than 30 minutes was confirmed. The insulating gas species were checked and $SF_6$ and $N_2$ gas produced good results with the Teflon insulator.

These steady state technology developments must be useful for future fusion devices since they were fully incorporated in the design of the LHD heating system.

## ACKNOWLEDGMENTS

The authors wish to thank Profs. A. Iiyoshi, M. Fujiwara, O. Motojima and K. Ohkubo for their helpful discussions and support.

## REFERENCES


1. A.IIYOSHI, K.YAMAZAKI, "The Next Large Helical Devices," *Physics of Plasmas*, **2**(6), 2349 (1995)

2. O.MOTOJIMA, K.AKAISHI, K.FUJII, et.al., "Physics and Engineering Design Studies on the Large Helical Device," *Fusion Engineering and Design* **20**, 3 (1993)

3. M.FUJIWARA, K.YAMAZAKI, M.OKAMOTO, et.al., "Large Helical Device (LHD) Program," *Journal of Fusion Energy*, **15**, 7 (1996)

4. T.MUTOH, R.KUMAZAWA, T.SEKI, et.al., "Development of steady-state ICRF heating for LHD", *Fusion Engineering and Design*, **26**, 387 (1995).

5. R.KUMAZAWA, T.WATARI, T.MUTOH, et.al., "Feedback Control Matching System for Temporal Change of Plasma Loading Resistance in High Power/Steady State ICRF Heating on the Large Helical Device", *Proceedings of 17h Symposium on Fusion Technology, ( 14-18 1992, Rome), ENEA Frascati*, **1**, 554, ( 1991).

6. T.MUTOH, R.KUMAZAWA, T.SEKI, et.al., "Development of Steady State ICRF Heating for Large Helical Device", *Proceedings of 16th Symposium on Fusion Engineering*, **2**, 1078, (1995).

7. R.KUMAZAWA, T.MUTOH, T.WATARI, et.al., "Achievement of 1.6MW/5000sec Operation of RF Oscillator on the Large Helical Device", *Proceedings of 19h Symposium on Fusion Technology*, **1**, 617, (1996).

8. T.MUTOH, R.KUMAZAWA, T.SEKI, et.al., "R&D of Steady State and High Voltage ICRF Transmission Line and Ceramic Feedthrough for LHD", *Proceedings of 17th Symposium on Fusion Engineering*, (1997) ,

9. N.GREENOUGH, G.GROTZ, "High Voltage RF Coaxial Vacuum Bushing Design Considerations", *Proceedings of 9th Symposium on Engineering Problems of Fusion Research*, **1**,844,(1981).

10. F.W.BAITY, W.E.BRYAN, D.J.HOFFMAN, et.al., "ICRF Antenna and Feedthrough Development at ORNL", *Proceedings of 11th Symposium on Fusion Engineering*. **2**, 1332, (1985).

11. T.L.OWENS, F.W.BAITY,D.J.HOFFMAN, et.al., "Radio Frequency Vacuum Feedthroughs for High-Power ICRF Heating Applications", *Fusion Technology*, **8**,381,(1985).

12. H.WEDLER, F.WESNER, W.BECKER, R.FRITSCH, "Vacuum Insulated Antenna Feeding Lines for ICRH at ASDEX Uprgade", *Fusion Engineering and Design*, **24**, 75, (1994).

13. M.SAIGUSA, T.FUJII, H.KIMURA, S.MORIYAMA, et.al., " Electrical Design and Test of ICRF Antenna for JT-60U", *Fusion Engineering and Design*, **24**, 47, (1994).

14. T.FUJII, M.SAIGUSA, H.KIMURA, S.MORIYAMA, et.al., "Performance of the JT-60 ICRF Antenna with an Open Type Faraday Shield", *Fusion Engineering and Design*, **19**, 213, (1992).

15. S.W.FERGUSON, R.W.CALLIS, W.P.CARY, et.al., "RF High Voltage Performance of RF Transmission Line Components on the DIII-D Fast Wave Current Drive (FWCD) System", *Proceedings of 16th Symposium on Fusion Engineering*, **1**, 837, (1995).

16. T.SHIMOZUMA, S.MORIMOTO, M.SATO, et.al., "A Forced Gas-Cooled Single-Disk Window Using Silicon Nitride Composite for High Power CW Millimeter Waves", *International Journal of Infrared and Millimeter Waves*, **18**, 1479, (1997).

Table 1. Dissipation Power Calculation and Comparison with the Experimental Results

| Type | Peak Power ($W/cm^3$) | Average Power ($W/cm^3$) | RF Voltage for Damage | RF Voltage for 30min. |
|---|---|---|---|---|
| Cylinder | 0.98 | 0.3 | ---- | 43 kV |
| Cone | 1.15 | 0.2 | ---- | 38 kV |
| Disk | 6.86 | 1.5 | 24 kV | 21 kV |
| Crank | 3.62 | 1.2 | 33 kV | 17 kV |

**Figure Captions**

Fig.1 Layout of the ICRF test stand set for the test of ceramic feedthrough and co-axial transmission lines. Ceramic feedthrough was set on the top of the test vacuum chamber. Cooling gas was circulated between gas injection ports on the feedthrough and bottom port on the left side of the 2nd stub tuner. For the test of co-axial transmission line, circuit was terminated at the point A. Co-axial line has 240 mm diameter and characteristic impedance of 50 Ohm. Inner conductor was cooled by circulating water flowing inside.

Fig.2 Drawings of the tested ceramic feedthroughs. All feedthroughs were connected to the co-axial transmission line of 240mmϕ diameter. Crank, disk and cone types consist of alumina ceramics and cylinder type consists of silicon nitride composites ceramic. Cone type has gas injection nozzles and a view port for the diagnostics. The vacuum seal method between ceramic and metal is O-ring for the cylinder type and brazing for others.

Fig.3 Tested RF voltages for the various types of ceramic feedthroughs in pulse and CW operations. Black rectangles show the records of the 30 minutes operations and white rectangles show the records of the 10 seconds operations. After the operations, vacuum leaks were happened for disks and crank types on the voltages shown by asterisks.

Fig.4 Photographs of the tested ceramic feedthroughs. (a) Cone type ceramic feedthrough and its inner conductor. Gas cooling nozzles are seen on the outside of the outer conductor. (b) All parts of the cylinder type feedthrough are shown. Ceramic material is silicon nitride composite having gray color. It has demountable structure using O-ring seal to avoid the crack on the brazing seal.

Fig.5 Measurements of the ceramic surface temperature of the cone type feedthrough, (a) by changing the RF voltage, and (b) by changing the gas flow rate to cool the ceramic surface. Gas flow rate were changed with the constant RF voltage at 30 $kV_{0\text{-}P}$. Each temperature increments are the data of after 30 minutes operations.

Fig.6 Temporal behaviors of the ceramic temperature with and without gas cooling in the cone type feedthrough. Nitrogen gas of 0.4MPa was circulated by the flow rate of 330 l/minute. RF voltage on the ceramic was 30-32 $kV_{0P}$.

Fig.7 The ANSYS code calculations of RF heat dissipation in the feedthrough ceramics estimated by Eq.(2) are shown by the contour line plots. The RF voltage between conductors is 50 $kV_{0P}$, the frequency is 50 MHz, the dielectric constant ratio is 9.7 and the loss tangent is 0.0002. The darkness of the contour plot areas are relative expressions and the absolute values of the RF dissipation power ($W/m^3$) are shown in the figures.

Fig.8 (a),(b) Drawings of the newly designed co-axial transmission line for steady state and high voltage operation. Cooling water flows inside the center conductors and the insulation gas circulates through the holes of Teflon spacers. The recess structures of the Teflon spacers at the corner edge of conductors to reduce the local electric field strength and the O-ring seal for watertight and contact fingers are shown in the elongated figure (b).

Fig.9 Photograph of the connectors of the co-axial transmission lines drawn in Fig.8. These co-axial lines were used for the feedthrough test and the high voltage steady state test of the transmission line with several insulation gas species.

Fig.10 High voltage test of the co-axial transmission line with different kinds of insulating gases. Black rectangles show the records of the steady state operations (30 minutes or 2 minutes) and white rectangles show the records of the 10 seconds operations. Filling gas pressure was 0.4 MPa.

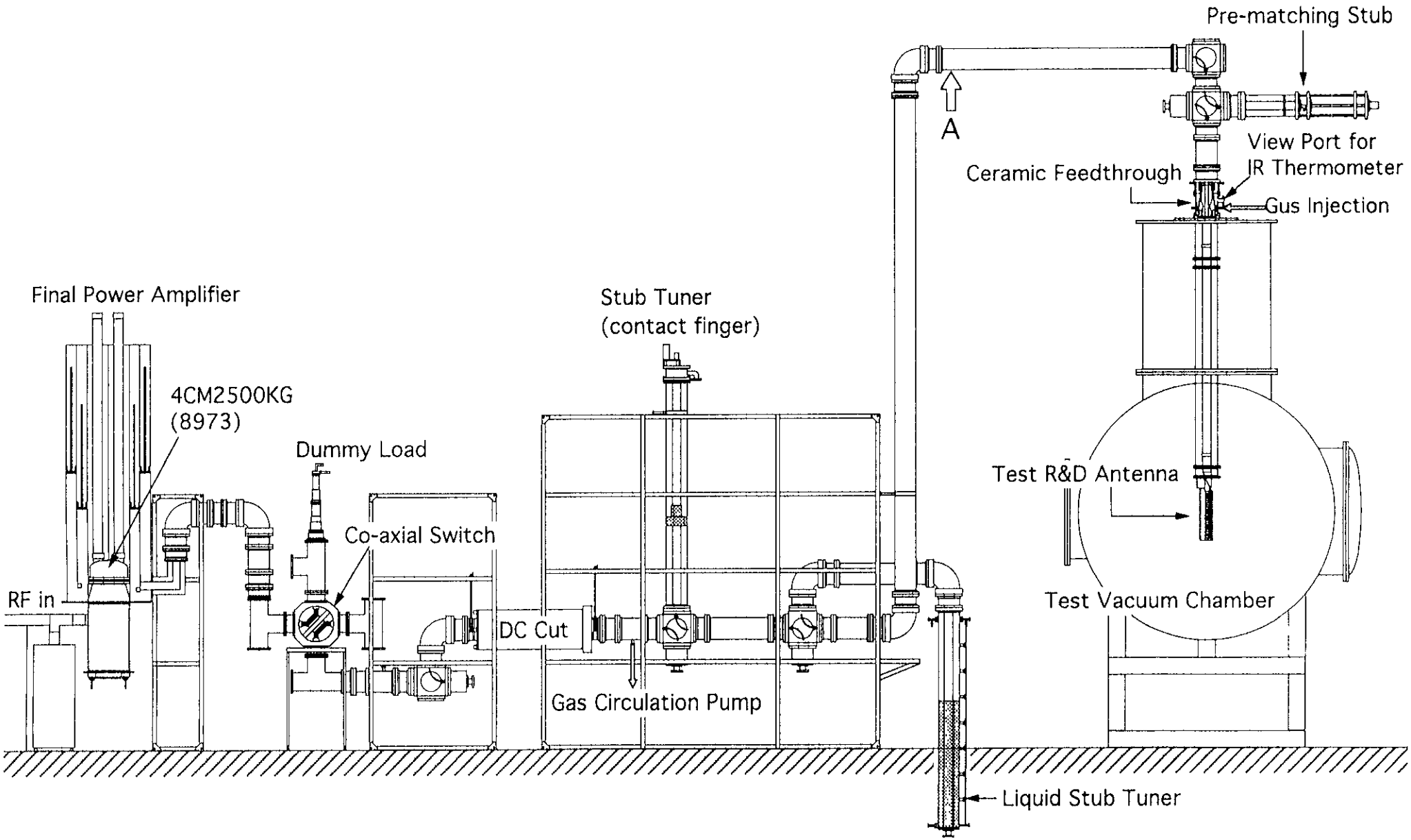


# Layout of ICRF Test Stand Set

Fig. 1

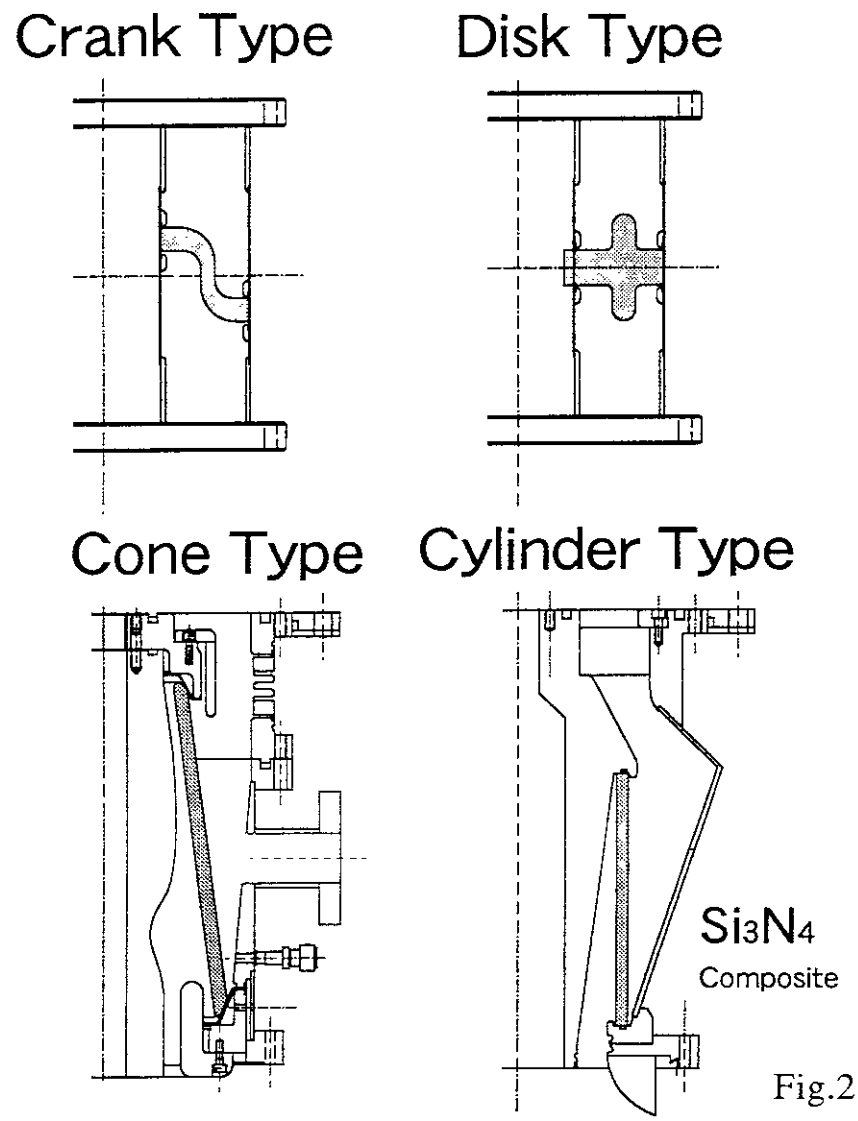
Crank Type
Disk Type
Cone Type
Cylinder Type
Si3N4
Composite

Fig.2

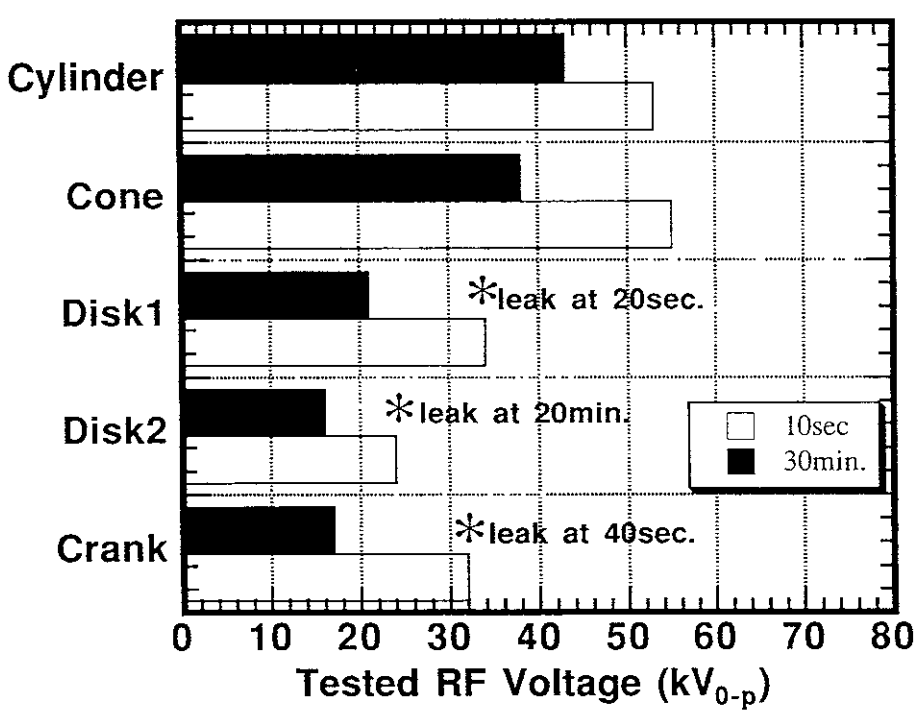
Cylinder
Cone
Disk1
Disk2
Crank
*leak at 20sec.
*leak at 20min.
*leak at 40sec.
10sec
30min.
0
10
20
30
40
50
60
70
80
Tested RF Voltage (kV0-p)

Fig.3

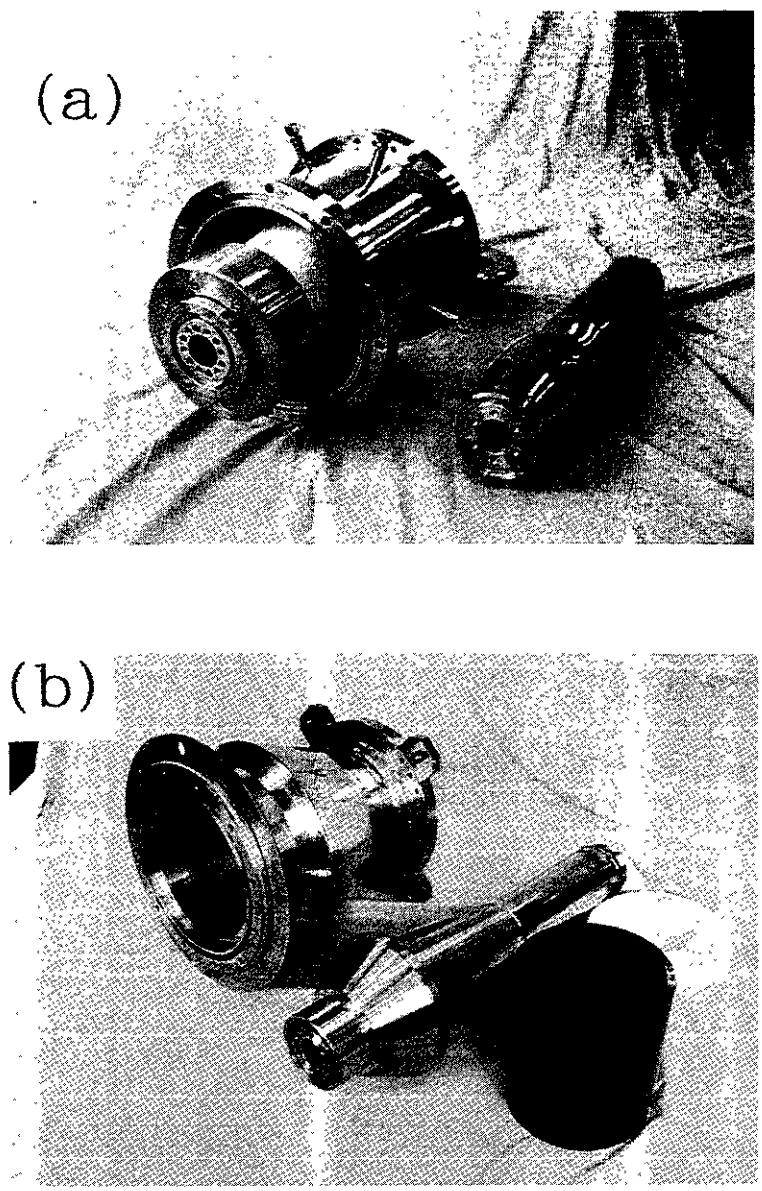


Fig.4

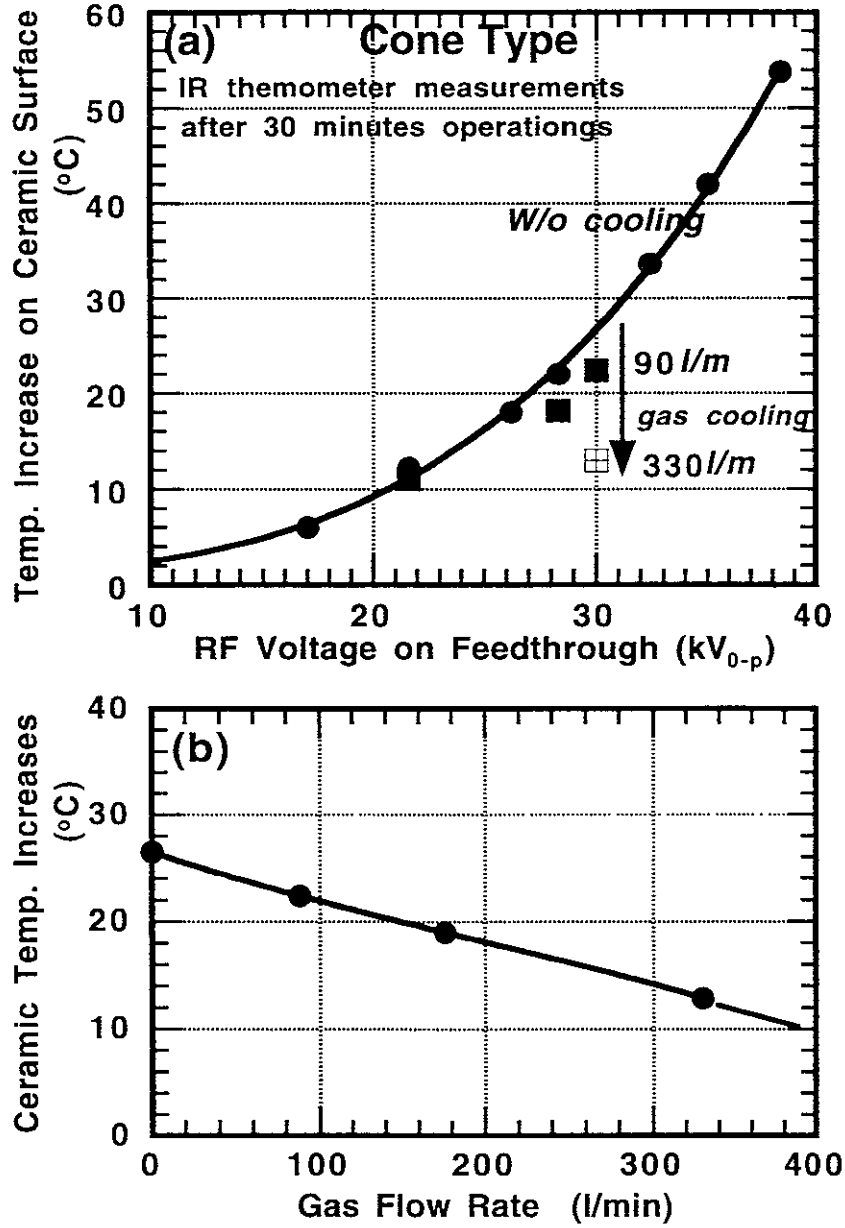
(a)
Cone Type
IR themometer measurements
after 30 minutes operationgs
W/o cooling
90 l/m
gas cooling
330 l/m
Temp. Increase on Ceramic Surface (°C)
RF Voltage on Feedthrough ($kV_{0-p}$)
(b)
Ceramic Temp. Increases (°C)
Gas Flow Rate (l/min)

Fig.5

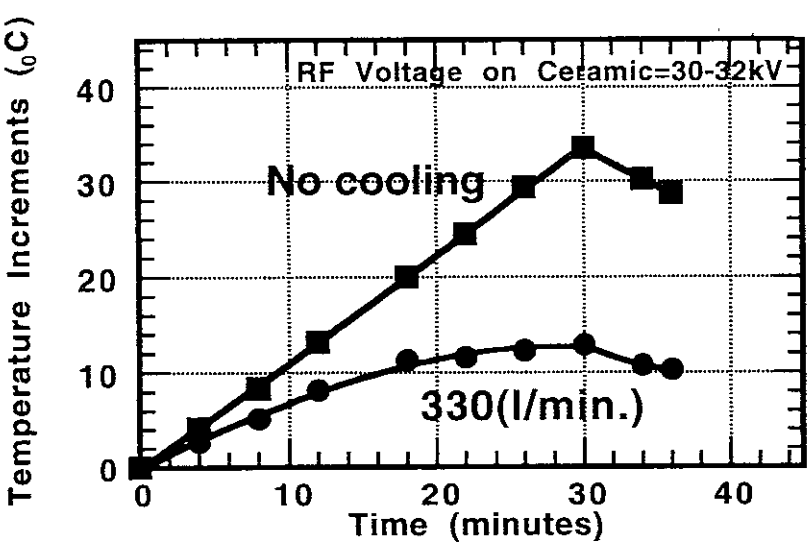
RF Voltage on Ceramic=30-32kV
No cooling
330(l/min.)
Temperature Increments ($_0$C)
Time (minutes)

Fig.6

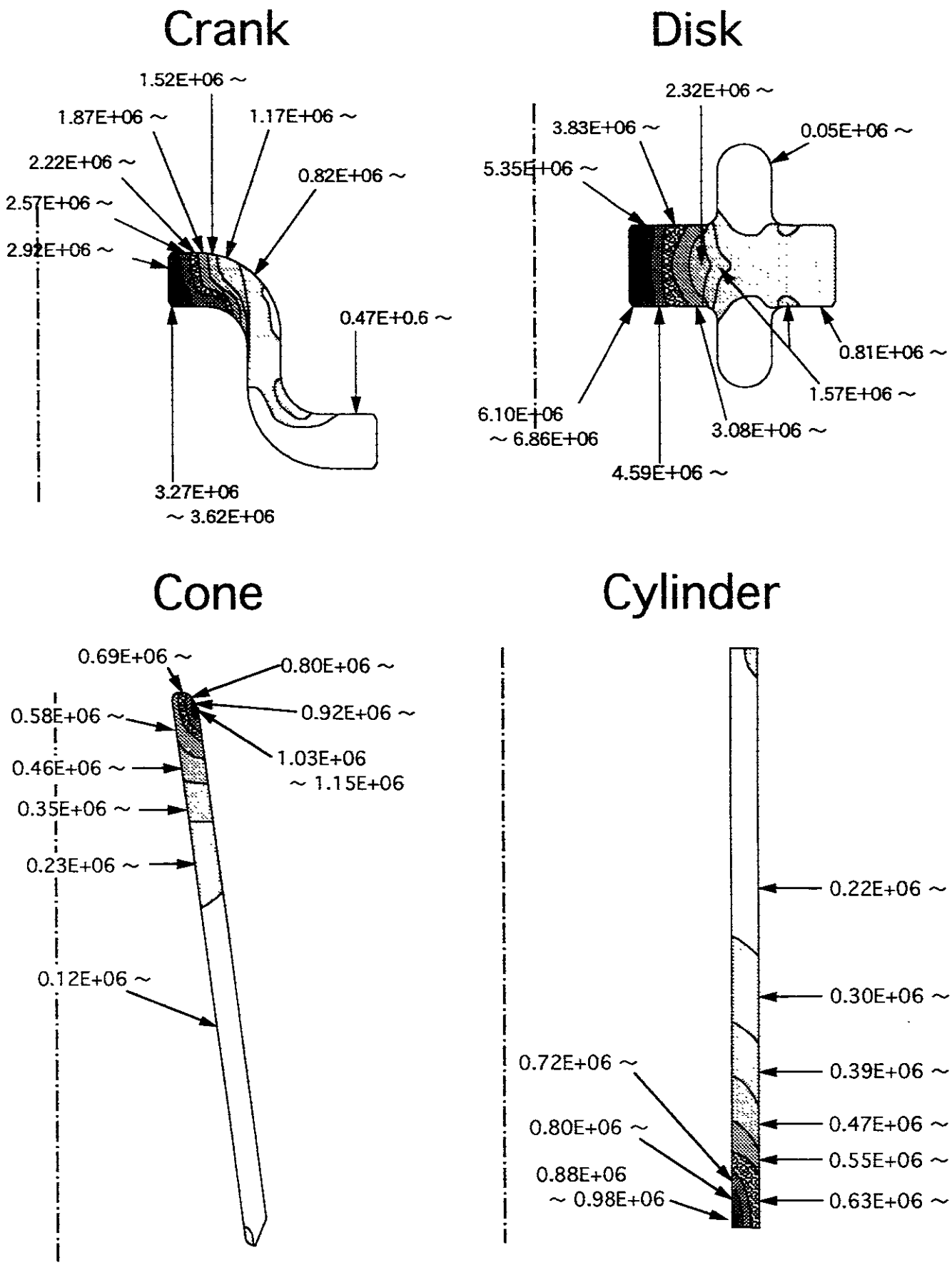
Crank
1.52E+06 ~
1.87E+06 ~
1.17E+06 ~
2.22E+06 ~
0.82E+06 ~
2.57E+06 ~
2.92E+06 ~
0.47E+0.6 ~
3.27E+06
~ 3.62E+06
Disk
2.32E+06 ~
3.83E+06 ~
0.05E+06 ~
5.35E+06 ~
0.81E+06 ~
1.57E+06 ~
6.10E+06
~ 6.86E+06
3.08E+06 ~
4.59E+06 ~
Cone
0.69E+06 ~
0.80E+06 ~
0.58E+06 ~
0.92E+06 ~
1.03E+06
~ 1.15E+06
0.46E+06 ~
0.35E+06 ~
0.23E+06 ~
0.12E+06 ~
Cylinder
0.22E+06 ~
0.30E+06 ~
0.72E+06 ~
0.39E+06 ~
0.47E+06 ~
0.80E+06 ~
0.55E+06 ~
0.88E+06
~ 0.98E+06
0.63E+06 ~

Fig.7

(a)

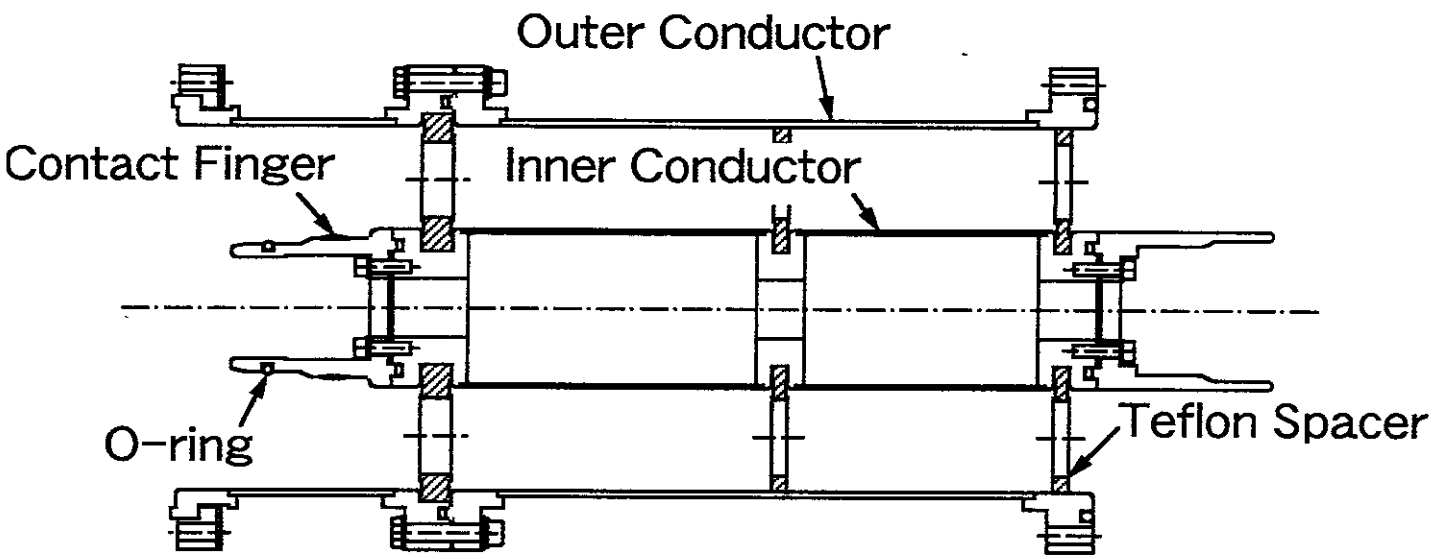
Outer Conductor
Contact Finger
Inner Conductor
O-ring
Teflon Spacer

(b)

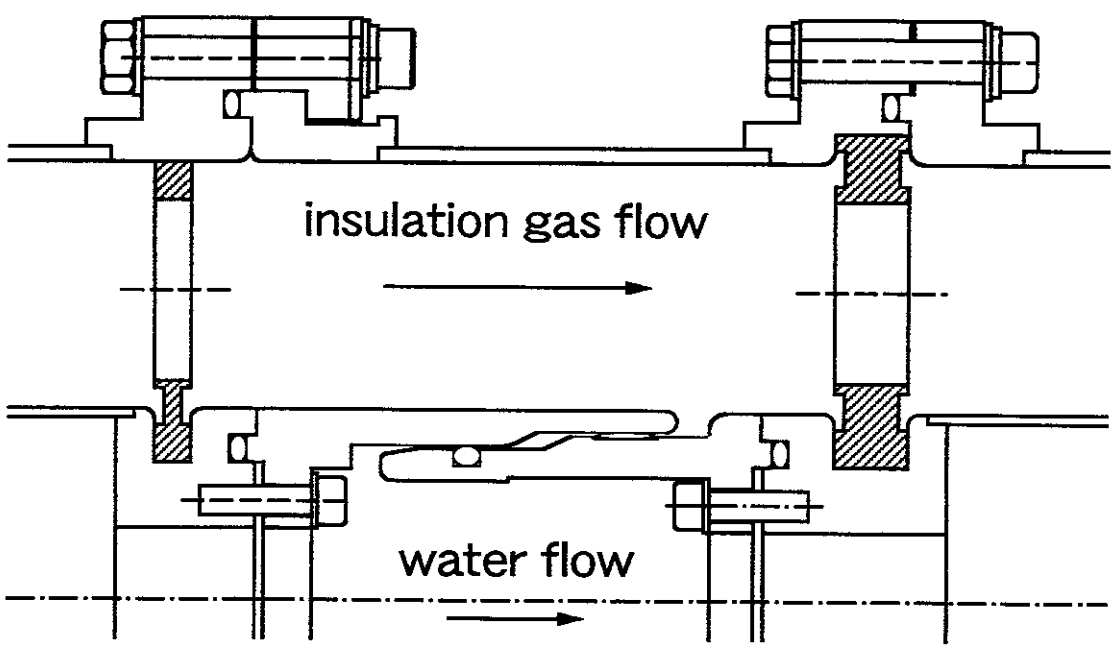
insulation gas flow
water flow

Fig.8

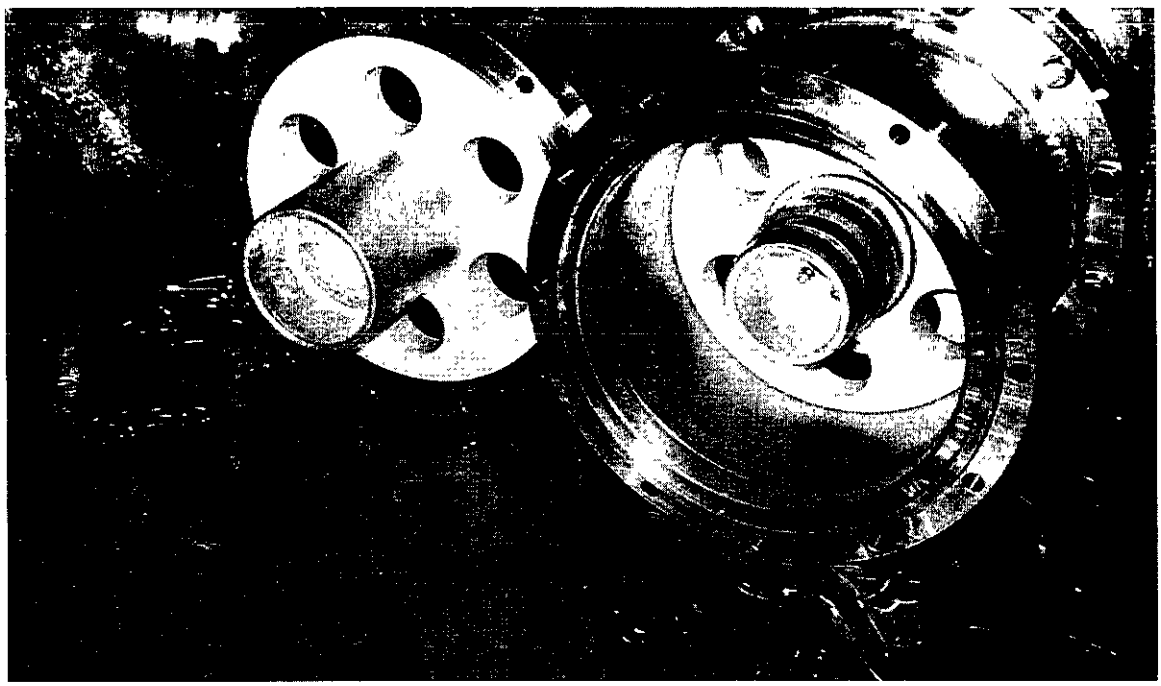

Fig.9

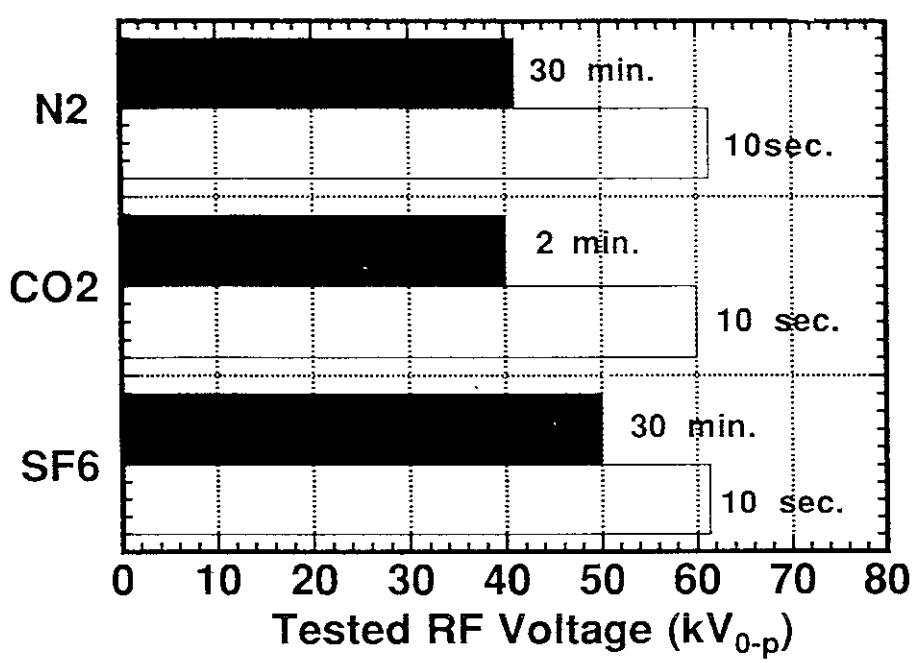
N2
30 min.
10sec.
CO2
2 min.
10 sec.
SF6
30 min.
10 sec.
0
10
20
30
40
50
60
70
80
Tested RF Voltage (kV0-p)

Fig.10

## Recent Issues of NIFS Series

NIFS-516 *Papers Presented at the 6th H-mode Workshop (Seeon, Germany)*; Oct 1997

NIFS-517 John L. Johnson,
*The Quest for Fusion Energy*; Oct 1997

NIFS-518 J. Chen, N. Nakajima and M. Okamoto,
*Shift-and-Inverse Lanczos Algorithm for Ideal MHD Stability Analysis*; Nov 1997

NIFS-519 M Yokoyama, N. Nakajima and M. Okamoto,
*Nonlinear Incompressible Poloidal Viscosity in L=2 Heliotron and Quasi-Symmetric Stellarators*; Nov. 1997

NIFS-520 S. Kida and H. Miura,
*Identificaiton and Analysis of Vortical Structures*, Nov. 1997

NIFS-521 K. Ida, S. Nishimura, T. Minami, K. Tanaka, S Okamura, M. Osakabe, H. Idei, S Kubo, C. Takahashi and K Matsuoka,
*High Ion Temperature Mode in CHS Heliotron/torsatron Plasmas*, Nov. 1997

NIFS-522 M Yokoyama, N Nakajima and M. Okamoto,
*Realization and Classification of Symmetric Stellarator Configurations through Plasma Boundary Modulations*; Dec. 1997

NIFS-523 H. Kitauchi,
*Topological Structure of Magnetic Flux Lines Generated by Thermal Convection in a Rotating Spherical Shell;* Dec. 1997

NIFS-524 T Ohkawa,
*Tunneling Electron Trap*, Dec. 1997

NIFS-525 K. Itoh, S.-I Itoh, M Yagi, A. Fukuyama,
*Solitary Radial Electric Field Structure in Tokamak Plasmas*, Dec 1997

NIFS-526 Andrey N. Lyakhov,
*Alfven Instabilities in FRC Plasma*, Dec. 1997

NIFS-527 J. Uramoto,
*Net Current Increment of negative Muonlike Particle Produced by the Electron and Posititve Ion Bunch-method*, Dec. 1997

NIFS-528 Andrey N Lyakhov,
*Comments on Electrostastic Drift Instabilities in Field Reversed Configuraiton*; Dec 1997

NIFS-529 J. Uramoto,
*Pair Creation of Negative and Positive Pionlike (Muonlike) Particle by Interaction between an Electron Bunch and a Positive Ion Bunch*; Dec. 1997

NIFS-530 J Uramoto,
*Measuring Method of Decay Time of Negative Muonlike Particle by Beam Collector Applied RF Bias Voltage*, Dec. 1997

NIFS-531 J. Uramoto,
*Confirmation Method for Metal Plate Penetration of Low Energy Negative Pionlike or Muonlike Particle Beam under Positive Ions*; Dec 1997

NIFS-532 J. Uramoto,
*Pair Creations of Negative and Positive Pionlike (Muonlike) Particle or K Mesonlike (Muonlike) Particle in H2 or D2 Gas Discharge in Magnetic Field*, Dec 1997

NIFS-533 S. Kawata, C Boonmee, T Teramoto, L. Drska, J. Limpouch, R. Liska, M. Sinor,
*Computer-Assisted Particle-in-Cell Code Development*; Dec. 1997

NIFS-534 Y. Matsukawa, T. Suda, S. Ohnuki and C. Namba,
*Microstructure and Mechanical Property of Neutron Irradiated TiNi Shape Memory Alloy*; Jan. 1998

NIFS-535 A. Fujisawa, H. Iguchi, H. Idei, S. Kubo, K. Matsuoka, S. Okamura, K. Tanaka, T. Minami, S. Ohdachi, S. Morita, H. Zushi, S. Lee, M. Osakabe, R. Akiyama, Y. Yoshimura, K. Toi, H. Sanuki, K. Itoh, A. Shimizu, S. Takagi, A. Ejiri, C. Takahashi, M. Kojima, S. Hidekuma, K. Ida, S. Nishimura, N. Inoue, R. Sakamoto, S.-I. Itoh, Y. Hamada, M. Fujiwara,
*Discovery of Electric Pulsation in a Toroidal Helical Plasma*; Jan. 1998

NIFS-536 Lj.R. Hadzievski, M.M. Skoric, M. Kono and T. Sato,
*Simulation of Weak and Strong Langmuir Collapse Regimes*; Jan. 1998

NIFS-537 H. Sugama, W. Horton,
*Nonlinear Electromagnetic Gyrokinetic Equation for Plasmas with Large Mean Flows*; Feb 1998

NIFS-538 H. Iguchi, T.P. Crowley, A. Fujisawa, S. Lee, K. Tanaka, T. Minami, S. Nishimura, K. Ida, R. Akiyama, Y. Hamada, H., Idei. M. Isobe, M. Kojima, S. Kubo, S Morita, S. Ohdachi, S. Okamura, M. Osakabe, K. Matsuoka, C. Takahashi and K. Toi,
*Space Potential Fluctuations during MHD Activities in the Compact Helical System (CHS);* Feb. 1998

NIFS-539 Takashi Yabe and Yan Zhang,
*Effect of Ambient Gas on Three-Dimensional Breakup in Coronet Formation Process*; Feb. 1998

NIFS-540 H. Nakamura, K. Ikeda and S. Yamaguchi,
*Transport Coefficients of InSb in a Strong Magnetic Field*; Feb. 1998

NIFS-541 J. Uramoto,
*Development of $\nu_\mu$ Beam Detector and Large Area $\nu_\mu$ Beam Source by $H_2$ Gas Discharge (I)*; Mar 1998

NIFS-542 J. Uramoto,
*Development of $bar\{\nu\}_\mu$ Beam Detector and Large Area $bar\{\nu\}_\mu$ Beam Source by $H_2$ Gas Discharge (II)*; Mar 1998

NIFS-543 J. Uramoto,
*Some Problems inside a Mass Analyzer for Pions Extracted from a $H_2$ Gas Discharge*; Mar. 1998

NIFS-544 J Uramoto,
*Simplified $\nu_\mu$ $bar\{\nu\}_\mu$ Beam Detector and $\nu_\mu$ $bar\{\nu\}_\mu$ Beam Source by Interaction between an Electron Bunch and a Positive Ion Bunch*; Mar. 1998

NIFS-545 J. Uramoto,
*Various Neutrino Beams Generated by $D_2$ Gas Discharge;* Mar 1998

NIFS-546 R. Kanno, N. Nakajima, T. Hayashi and M. Okamoto,
*Computational Study of Three Dimensional Equilibria with the Bootstrap Current*; Mar. 1998

NIFS-547 R. Kanno, N. Nakajima and M. Okamoto,
*Electron Heat Transport in a Self-Similar Structure of Magnetic Islands;* Apr 1998

NIFS-548 J.E. Rice,
*Simulated Impurity Transport in LHD from MIST;* May 1998

NIFS-549 M.M. Skoric, T. Sato, A.M. Maluckov and M.S. Jovanovic,
*On Kinetic Complexity in a Three-Wave Interaction;* June 1998

NIFS-550 S. Goto and S. Kida,
*Passive Saclar Spectrum in Isotropic Turbulence: Prediction by the Lagrangian Direct-interaction Approximation;* June 1998

NIFS-551 T. Kuroda, H. Sugama, R. Kanno, M. Okamoto and W. Horton,
*Initial Value Problem of the Toroidal Ion Temperature Gradient Mode ;* June 1998

NIFS-552 T. Mutoh, R. Kumazawa, T. Seki, F. Simpo, G. Nomura, T. Ido and T. Watari,
*Steady State Tests of High Voltage Ceramic Feedthoughs and Co-Axial Transmission Line of ICRF Heating System for the Large Helical Device ;* June 1998